Available online at www.sciencedirect.com
SCIENCE DIRECT®
Journal of Electroanalytical Chemistry xxx (2005) xxx–xxx
Journal of Electroanalytical Chemistry
www.elsevier.com/locate/jelechem

Understanding the anatomy of capacitance at interfaces between two immiscible electrolytic solutions

C.W. Monroe [a], M. Urbakh [b], A.A. Kornyshev [a,*]

[a] Department of Chemistry, Faculty of Physical Sciences, Imperial College, London SW72AZ, UK
[b] School of Chemistry, Tel Aviv University, Ramat Aviv, 69978 Tel Aviv, Israel

Received 28 February 2005; received in revised form 16 April 2005; accepted 18 April 2005

This paper is dedicated to Ron Fawcett on the occasion of his 65th birthday

Abstract

Why does the Gouy–Chapman theory often predict the magnitude and behavior of capacitance curves at the interface between two immiscible electrolytic solutions, and sometimes fail? Why do experiments sometimes show an "unphysical" negative or zero Stern-layer contribution to the inverse capacitance? These questions motivated the construction of a model to encapsulate the anatomy of this easily experimentally accessible interfacial characteristic. The Verwey–Niessen theory is extended here to allow ionic penetration at the interface. This extension explains several features of experimental curves that arise when solutes vary, such as asymmetry and shifts of the capacitance minimum – features that are described by neither the Gouy–Chapman nor the Verwey–Niessen theories. Free energies of ion transfer are taken as model input parameters to describe ionic penetration into a mixed-solvent interfacial layer. With a single additional parameter that lies in a narrowly constrained range, the model successfully reproduces experimental data. It also shows why the Gouy–Chapman theory works and why the Verwey–Niessen theory rarely does, rationalizing how inner-layer contributions are hidden in the capacitance response.

1. Introduction

The past decade has witnessed a significant increase of research interest in the study of interfaces between two immiscible electrolytic solutions (ITIES), fueled in part by new experimental and theoretical methods [1–4]. Systems based on the liquid–liquid interface have drawn much attention; ITIES have structural and dynamic properties unobserved in bulk liquids and are integral to many chemical, biological, and biomimetic systems. These interfaces are important in various practical applications, such as phase-transfer catalysis, solvent extraction, and ion-selective electrode operation. They also provide a defect-free junction for studying adsorption phenomena, charge-transfer reactions, and phase-formation processes. ITIES are chargeable due to the presence of back-to-back double layers; the electric fields localized at the solvent junction offer unique opportunities to influence processes at and properties of the interface.

Early models applied to classical experiments such as differential-capacitance and electrocapillary measurements have depicted the interface as two space–charge regions, either with a sharp impenetrable boundary or separated by a compact inner layer of solvent molecules [5–10]. These models have been widely applied to ITIES, although there remains some controversy regarding the nature of the inner layer [11–13]. In particular, it remains unclear why Parsons–Zobel plots [14,15] do not consistently show an inner-layer contribution to inverse capacitance.

* Corresponding author. Tel.: +44 20 759 45786; fax: +44 20 759 45801.
E-mail address: a.kornyshev@imperial.ac.uk (A.A. Kornyshev).

0022-0728/$ - see front matter © 2005 Published by Elsevier B.V.
doi:10.1016/j.jelechem.2005.04.031

Nomenclature

Roman

$a^{\theta}_{i,j}$	potential- and concentration-independent secondary reference state for the activity of species i from phase j
C_{ITIES}	area-specific capacitance of the ITIES (F/m^2)
c^j_i	concentration of species i in diffuse layer j (mol/m^3)
c^j_0	bulk concentration of neutral electrolyte in phase j (mol/m^3)
d	inner-layer thickness (m)
e	elementary charge, 1.60×10^{-19} C
F	Faraday's constant, 96,487 C/equiv
$\Delta G^{j,k}_i$	free energy of transfer for species i from phase j to phase k (J/mol)
$\Delta G^{\mathrm{IHP}}_{i,j}$	free energy cost for species i from phase j to reach IHP (J/mol)
IHP	inner Helmholtz plane depicted in Figs. 1 and 2
ITIES	the interface between two immiscible electrolytic solutions
K^j_i	equilibrium constant for mixed-layer penetration of species i from phase j (m^3/mol)
$\mathscr{K}$	dimensionless function defined by Eq. (15)
$\mathscr{K}^j_i$	dimensionless equilibrium constant for mixed-layer penetration by species i from phase j
M^j_+	chemical symbol of a cation from phase j
MD	molecular dynamics
N_{A}	Avogadro's number, 6.022×10^{23} mol^{-1}
n_{s}	saturation number defined by Eq. (13)
NB	nitrobenzene
OHP	outer Helmholtz planes depicted in Figs. 1 and 2
ODDL	outer diffuse double layer depicted in Fig. 1
$\mathscr{Q}$	dimensionless surface charge on IHP defined by Eq. (3)
q^{II}	charge contribution from semispace II (C/m^2)
q^{IHP}	surface charge on IHP (C/m^2)
R	gas constant, 8.3143 J/mol K
r	mean radius of interacting ions (m)
T	absolute temperature (K)
TBATPB	tetrabutylammonium tetraphenylborate
X^j_-	chemical symbol of an anion from phase j
z	equivalent ionic charge, defined to be positive (equiv/mol)

Greeks

α	transfer fraction defined by Eq. (5)
$\beta_{i,km}$	interaction free energy between species k from phase m and species i (J/mol)
Γ_{T}	total surface concentration of available penetration sites (mol/m^3)
γ	ratio of dielectric constants defined by Eq. (2)
ϵ_0	permittivity of free space, 8.85×10^{-12} (F/m)
ϵ^j	dielectric constant of solvent in phase j
ϵ^{eff}	effective dielectric constant when ions interact
ζ	ratio of Debye lengths defined by Eq. (2)
$\Theta_{i,j}$	fractional surface penetration of species i native to phase j on surface IHP
λ^j	Debye length in phase j (m)
ν	stoichiometric number of ions in the symmetric salts
ϖ	dimensionless function defined by Eq. (14)
Φ	electrostatic potential (V)
ϕ	dimensionless potential, defined similarly to $\Delta\phi$
$\Delta\phi$	dimensionless potential drop across the ITIES defined by Eq. (3)
$\Delta\phi^{\mathrm{int}}$	dimensionless potential drop across the mixed inner layer
χ	dimensionless inner-layer capacitance defined by Eq. (2)

Symbols and superscripts

*	chemical symbol of an available penetration site on the interface
I phase	at the right of Fig. 1
II phase	at the left of Fig. 1
int phase	at the center of Fig. 1
+o	cations from the organic phase
−o	anions from the organic phase
+w	cations from the aqueous phase
−w	anions from the aqueous phase

Recently, the structure of and kinetics at the ITIES have been under close examination by spectroscopic and optical techniques [1,16–18]. Several analytical methods have also been applied to describe the chemical physics of the ITIES. Molecular dynamics (MD) and Monte Carlo simulations by Benjamin suggest that the interface is molecularly sharp, with capillary waves extending over 1 nm [3,19]. However, MD computations focus mainly on the neat molecular interface or interfaces with few ions present. Computer simulations have been extended to more complex systems by employing the lattice gas model, which is a useful theoretical approach to describe space–charge regions, adsorption, and kinetics at the interface [2,20,21]. In addition, theoretical approaches based on a continuüm description of the interfacial region have been developed to include the effects of capillary waves, ionic penetration and ionic association [22,4,12].

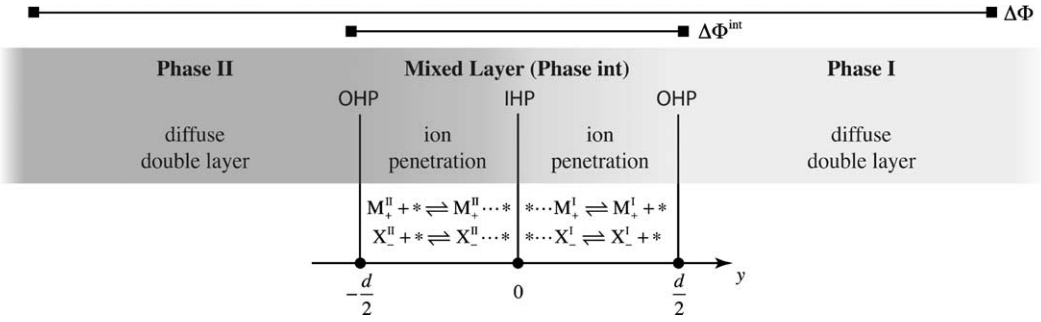

Fig. 1. Schematic of the interface between immiscible electrolytic solutions (ITIES).

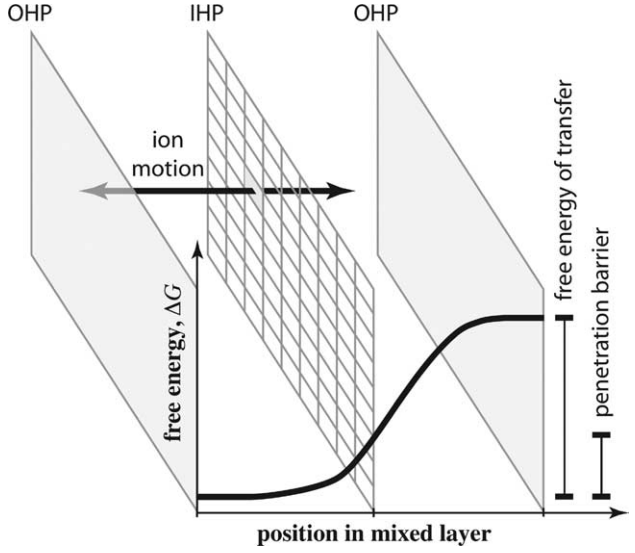

Fig. 2. Sketch representing the idealization of a mixed-layer penetration event.

The ideas of ion penetration and a special interfacial layer are not new. Torrie and Valleau [23] suggested a primitive model in which penetration of ions close to the interface was controlled by image forces but did not introduce an inner layer with distinct properties. Samec et al. [24] were the first to incorporate a separate inner layer. In their model, only organic ions were allowed to enter the inner region and no free energy of transfer from the bulk to the inner layer was considered. In addition, the model introduced a separate empirical "Debye length" in the inner region, a parameter that cannot be rationalized physically on that short length scale. Only the linearized Poisson–Boltzmann response was used, limiting the results to polarizations near the potential of zero charge. Schmickler et al. [25–27] have shown by analytical methods that an interfacial region of finite thickness into which ions penetrate explains enhancements of the capacitance from the Gouy–Chapman limit, and that ion association can rationalize asymmetries in the capacitance response. Very recently, the research group of Girault [28] also demonstrated that the charge distribution in the interfacial region can be affected by the adsorption of ionic species, which results in significant changes in the potential profiles across the interface. The same group found that the commonly observed characteristics of experimental capacitance–voltage curves can be explained by ionic adsorption at the interface.

In the present work, an idealized three-phase phenomenological model is developed to describe both penetration of and interactions between ionic species at the ITIES. As discussed below, the approach is basically similar to the one proposed by Su et al. [28], but it incorporates a number of new elements. The solvent junction is included as a distinct, mixed-dielectric region into which ions may penetrate; entry by all ions into the inner layer is also allowed. Impeded penetration, rather than an energetically favorable adsorption, is a central part of the model presented here. These two features were included similarly as in the model of Schmickler et al. [27]. However, this model has two principle differences. Thermodynamic ion-transfer data are directly employed and limit the model to a single adjustable parameter that varies within a narrow range. In addition, the simplified three-phase model presented here does not require numerical solution of a coupled system containing a nonlinear differential equation, and thus is computationally simpler.

Several experimental quantities are involved in the model without any special assumptions. Free energies of transfer for ionic species between solvent phases, as summarized in [29,30], are included to describe the energetics of ion penetration into the interfacial layer. In addition, the interfacial region is taken to have a finite thickness that corresponds to X-ray diffraction measurements [1] – a feature not present in the model by Su et al. [28]. The nitrobenzene–water interface has been very thoroughly characterized and is selected as an exemplary system for analysis here. As the model equations can be derived by standard methods, the paper contains minimal algebra. The primary emphasis will be on a qualitative description of the results, which are intended to provide experimentalists with a tool to interpret their capacitance data.

2. The basic model

Due to considerable observed potentials of zero charge [31,32] that cannot be explained by surface-dipole potential drops at the water/oil interface, it is often speculated that there must be some charge density at the equilibrated, unpolarized ITIES. Su et al. [28] have suggested the existence of a potential trap at the interface, showing that specific interactions involving a charged solute can explain the accumulation of interfacial charge without a potential bias. In fact, there are two types of specific phenomena that may impact the free energies of charged species near the boundary between solvents: solute–solute interactions and solute–solvent interactions.

Solute–solute interactions can be included in the model presented here; their role is addressed in a later section, where they are shown to be a secondary effect at low polarizations. Solute–solvent interactions are of primary importance. They are accounted for in this model by the ionic free energies of transfer. The free energies determine the milder or stronger exclusion of ions from the interface, but not attractions toward it. Differences in exclusive forces and the roughly concentration-independent dipolar potential drop are taken here to be the sources of the system capacitance signature. Thus, the model relies on a different physical conception than that typically applied to adsorption processes.

2.1. Model equations

Fig. 1 sketches the ITIES structure as it is considered in the model. The figure shows three phases, denoted by I, II, and int. Phases I and II are typical diffuse double layers containing well-solvated ions. Phase int is an inner layer of thickness d at the interface between the two immiscible solutions. The solvents may mix to some extent in the inner region, and, though it is energetically unfavorable, ions may also enter it. The penetration of ions from the phase in which they are well solvated into the opposing phase is neglected; this is a simplifying but quantitatively viable assumption because the statistical weight of the ions that go beyond the inner layer to the opposite phase is relatively small. Three dividing surfaces are marked on the figure. Those marked OHP denote outer Helmholz planes, the closest distance to which well-solvated ions approach the interface; IHP shows the inner Helmholz plane, which is the average position of ions that penetrate the mixed layer. For simplicity in the analysis, surface IHP is placed at the midpoint between surfaces OHP, and the diffuse double layers are taken to extend semi-infinitely in either direction.

To avoid terminological confusion, the terms "Gouy–Chapman model" and "Verwey–Niessen model" used throughout the paper should be clarified. Hereafter, the term "Gouy–Chapman model" refers to a physical situation in which the two back-to-back diffuse double layers, generally described by nonlinear Poisson–Boltzmann equations, meet at a plane impenetrable to ions. The "Verwey–Niessen model" differs from the Gouy–Chapman model in that there is a compact solvent layer between the diffuse double layers.[1]

In the diffuse double layers, the potential distribution is described by the nonlinear Poisson–Boltzmann equation. The inner layer is considered as two parallel-plate capacitors in series; in this sense, the derivation of the equations is very similar to that of the Verwey–Niessen model [10]. However, the solution to the electrostatic governing equations is modified slightly to allow charge accumulation at surface IHP. The dimensionless potential drop from phase II to phase I, $\Delta\phi = \phi^{\mathrm{II}} - \phi^{\mathrm{I}}$, is given by

$$\Delta\phi(\mathcal{Q},\Delta\phi^{\mathrm{int}}) = 2\ln\left[\frac{\gamma^2(\mathcal{Q}+\chi\Delta\phi^{\mathrm{int}})+\gamma\sqrt{\gamma^2\left(\mathcal{Q}+\chi\Delta\phi^{\mathrm{int}}\right)^2+16\zeta^2}}{\zeta^2(\mathcal{Q}-\chi\Delta\phi^{\mathrm{int}})+\zeta\sqrt{\zeta^2(\mathcal{Q}-\chi\Delta\phi^{\mathrm{int}})^2+16\gamma^2}}\right]+\Delta\phi^{\mathrm{int}}, \quad (1)$$

which is a function of the potential drop across phase int, $\Delta\phi^{\mathrm{int}}$, and the surface charge density on the IHP, $\mathcal{Q}$. Eq. (1) is derived under the conditions that both electrolytes have identical equivalent charges and are symmetrical.

The expression for potential drop in Eq. (1) contains several dimensionless quantities for brevity of notation. Eq. (1) is parameterized by the ratio of Debye lengths, ζ, a solvent dielectric constant ratio, γ, and the dimensionless inner-layer capacitance χ,

$$\zeta^2 = \frac{\lambda^{\mathrm{II}}}{\lambda^{\mathrm{I}}} = \sqrt{\frac{\epsilon^{\mathrm{II}}c_0^{\mathrm{I}}}{\epsilon^{\mathrm{I}}c_0^{\mathrm{II}}}}, \quad \gamma = \sqrt{\frac{\epsilon^{\mathrm{II}}}{\epsilon^{\mathrm{I}}}}, \quad \chi = \frac{2\epsilon^{\mathrm{int}}}{d}\sqrt{\frac{\lambda^{\mathrm{I}}\lambda^{\mathrm{II}}}{\epsilon^{\mathrm{I}}\epsilon^{\mathrm{II}}}}. \quad (2)$$

Here, ϵ^j, λ^j, and c_0^j are the dielectric constant, Debye length, and bulk salt concentration in phase j, respectively. In the model, the dielectric constant of the inner layer, ϵ^{int}, is considered to be constant and equal to the average of the solvent dielectric constants. The assumption that ϵ^{int} is constant is reasonable, because the maximum values of the electric field at the inner layer are insufficient to induce dielectric saturation. The potential drop and surface charge are defined dimensionlessly as

$$\Delta\phi = \frac{Fz\Delta\Phi}{RT}, \quad \mathcal{Q} = \frac{Fzq^{\mathrm{IHP}}}{RT\epsilon_0}\sqrt{\frac{\lambda^{\mathrm{I}}\lambda^{\mathrm{II}}}{\epsilon^{\mathrm{I}}\epsilon^{\mathrm{II}}}}, \quad (3)$$

[1] This second physical picture is often called the "modified Verwey–Niessen model", and was proposed by Gavach et al. [10].

where F is Faraday's constant, R is the gas constant, and ϵ_0 is the permittivity of free space; T is the absolute temperature, z the (positive) equivalent charge of the salt ions, Φ the electrostatic potential, and q^{IHP} the charge density on the inner dividing surface. The inner-layer potential drop, $\Delta\Phi^{\mathrm{int}}$, occurs between dividing surfaces OHP in Fig. 1. Its dimensionless form, $\Delta\phi^{\mathrm{int}}$, is defined similarly to the overall dimensionless potential drop $\Delta\phi$ given in Eq. (3).

Entrance of an ion into the inner layer is considered here to be an elementary, reversible, and equilibrated electrochemical reaction. Mechanisms for the four mixed-layer penetration reactions are shown beneath phase int in Fig. 1. Five chemical quantities are employed in the mechanisms: M^j_+ and X^j_-, respectively, denote cations and anions from bulk solution j, and $*$ represents a site through which an ion may penetrate surface IHP.

The idealization of a penetration event is shown in Fig. 2, which depicts dividing surface IHP as a plane lattice. The interstices in the grid represent sites available for ion penetration, denoted by $*$ in the penetration mechanisms shown in Fig. 1. In this analysis, the Langmuir condition is adopted; the total number of ion penetration sites is assumed independent of concentration and potential such that

$$1 = \Theta_{+,\mathrm{I}} + \Theta_{-,\mathrm{I}} + \Theta_{+,\mathrm{II}} + \Theta_{-,\mathrm{II}} + \Theta_{*,\mathrm{IHP}}, \tag{4}$$

where $\Theta_{*,\mathrm{IHP}}$ denotes the fractional surface coverage of available penetration sites on dividing surface IHP.

Fig. 2 also shows the energetics of an ion penetration reaction between dividing surfaces OHP. The double arrow in the figure represents a path an ion may travel over time due to random thermal motion. There is a free-energy cost for an ion to lose the shell of solvent in which it is naturally miscible and become solvated in the other phase. This cost, ΔG, is sketched as a function of position in the figure. The ion depicted is miscible in the left phase, as indicated by the free-energy barrier, which increases from left to right. Overall energy barriers for ions to lose their solvation shells in one phase and take on shells of another solvent are experimentally accessible. Thermodynamic measurements of ionic free energies of transfer abound in the literature [29,30,33–38]; the magnitude of the free energy of transfer for the penetrating ion is shown to the right of the free-energy profile in Fig. 2. It should be noted that the energy profile associated with the penetration of ions may not always be sigmoidal as depicted in Fig. 2; surfactant ions may adsorb at the ITIES and their energy profiles may not be monotonic across it. However, for the ions considered in this paper, which are geometrically symmetric, there is no grounds to expect that the energy profile has a minimum at the interface.

Dividing surface IHP is defined to reside at the center of phase int. At this plane, a penetrating ion has a free energy higher than in the bulk solution, but lower than its free energy of transfer. In the model, this relative free energy, $\Delta G^{\mathrm{IHP}}_{i,j}$, is expressed as a fraction, α, of the free energy of transfer. The free energy of a species on dividing surface IHP relative to its energy in the diffuse layer is given by

$$\Delta G^{\mathrm{IHP}}_{i,j} = \alpha \Delta G^{j,k}_i, \tag{5}$$

where $\Delta G^{\mathrm{IHP}}_{i,j}$ denotes the free energy cost for species i from phase j to reach dividing surface IHP and the free energy of transfer of species i from phase j to phase k is represented by $\Delta G^{j,k}_i$. Fig. 2 also shows the magnitude of the penetration barrier $\Delta G^{\mathrm{IHP}}_{i,j}$ to the right of the free-energy profile. In reality, there is a distribution of penetration energies because individual ions may cross the interface to varying extents. Thus, $\Delta G^{\mathrm{IHP}}_{i,j}$ should be interpreted as the average penetration-energy barrier for ions of a given type. Because surface IHP is at the center of phase int, it is expected that α should be less than or equal to 1/2. As a true input parameter, the transfer fraction α is independent of potential.[2] Free energies of transfer are different for each species, but random thermal fluctuations affect all ions equally; the transfer fractions may, in principle, be different for each ion. However, as a simplification to reduce the parameter space of the model, this quantity is taken to be identical for all species. Even with this assumption, the model successfully describes experimental results in a typical ITIES. In less ideal systems, where ions are asymmetric or behave as surfactants, differences in α may need to be considered from species to species. The exact values of $\Delta G^{\mathrm{IHP}}_{i,j}$ could be accessed by MD simulation.

Free-energy considerations between dividing surfaces can be taken into account by standard methods. The four penetration equilibria in the inner layer are incorporated into the model according to the electrochemical thermodynamic method presented by Newman and Thomas-Alyea [39], which accounts for reactions that occur between multiple dividing surfaces. For example, the penetration of cations from plane OHP in phase I (at position $d/2$) to dividing surface IHP (at position 0) is described by the relationship

$$K^{\mathrm{I}}_+ = \frac{\Theta_{+,\mathrm{I}}}{c^{\mathrm{I}}_+\big|_{d/2}\Theta_{*,\mathrm{IHP}}} \exp[-(\phi|_{d/2} - \phi|_0)]. \tag{6}$$

Here, K^{I}_+ is the equilibrium constant for mixed-layer penetration of cations from phase I, defined such that

[2] Although this analysis is restricted to ions at infinite dilution, α may also in general depend on the bulk electrolyte concentration. Surface tension lowers with bulk concentration; as the interface becomes less stiff, capillary fluctuations increase, the distance over which the free-energy barrier rises smears, and there is a lower energy cost for ions to penetrate the inner layer and reach the IHP [22]. This dependence is not considered explicitly here, but should be borne in mind.

it is zero if the species cannot enter phase int. To denote the ionic concentration and dimensionless potential at surface OHP, the symbols $c_+^{\mathrm{I}}|_{d/2}$ and $\phi|_{d/2}$ are employed; the variable. $\phi|_0$ represents the dimensionless potential at surface IHP.

Equilibrium constants for penetration are also related to the penetration-barrier free energies according to

$$K_i^j = a_{i,j}^{\theta} \exp\left(-\frac{\Delta G_{i,j}^{\mathrm{IHP}}}{RT}\right). \tag{7}$$

The quantity $a_{i,j}^{\theta}$ has units of inverse concentration, and represents a potential- and concentration-independent secondary reference state for the activity of species i from phase j. Here, an ideal-solution approximation is adopted, and $a_{i,j}^{\theta}$ is taken to be the inverse of the pure solvent concentration in phase j, $a_{i,j}^{\theta} = 1/c_{\mathrm{s}}^j$. A similar approximation was applied successfully in the single-species adsorption model presented by Su et al. [28]. Dimensionless equilibrium constants for the mixed-layer penetration of species i from phase j are defined by

$$\mathscr{K}_i^j = \nu c_0^j a_{i,j}^{\theta} K_i^j, \tag{8}$$

where ν represents the stoichiometric number of an ion in the neutral salt. The coefficient $\nu c_0^j a_{i,j}^{\theta}$ can be construed in the ideal-solution limit as the particle fraction of ions in the neutral bulk.

Equilibrium relations like Eq. (6) can be simplified due to the absence of faradaic processes at the inner layer. Near an ideally polarizable interface, the diffuse-layer ion concentrations. $c_i^j|_{\pm d/2}$ are Boltzmann distributed in potential. This relationship allows the concentrations of ions at OHP to be replaced with results from the electrostatic analysis. The equilibrium expressions for ion penetration become

$$\begin{aligned}
\Theta_{+,\mathrm{I}} &= \mathscr{K}_+^{\mathrm{I}} \Theta_{*,\mathrm{IHP}} \exp(-\Delta\phi^{\mathrm{I}}),\\
\Theta_{-,\mathrm{I}} &= \mathscr{K}_-^{\mathrm{I}} \Theta_{*,\mathrm{IHP}} \exp(\Delta\phi^{\mathrm{I}}),\\
\Theta_{+,\mathrm{II}} &= \mathscr{K}_+^{\mathrm{II}} \Theta_{*,\mathrm{IHP}} \exp(\Delta\phi^{\mathrm{II}}),\\
\Theta_{-,\mathrm{II}} &= \mathscr{K}_-^{\mathrm{II}} \Theta_{*,\mathrm{IHP}} \exp(-\Delta\phi^{\mathrm{II}})
\end{aligned} \tag{9}$$

These equations express the fractional surface penetrations through the potential drops in semispaces I and II, given by $\Delta\phi^{\mathrm{I}}$ and $\Delta\phi^{\mathrm{II}}$, respectively, and the dimensionless equilibrium constant $\mathscr{K}_i^j$. The potential drop in semispace I, which is the entire region to the right of IHP in Fig. 1, can be obtained through the solution of the electrostatic problem

$$\Delta\phi^{\mathrm{I}} = 2\ln\left[\frac{\gamma}{4\zeta}(\mathscr{Q} + \chi\Delta\phi^{\mathrm{int}}) + \sqrt{\frac{\gamma^2}{16\zeta^2}(\mathscr{Q} + \chi\Delta\phi^{\mathrm{int}})^2 + 1}\right] + \frac{1}{2}\Delta\phi^{\mathrm{int}} + \frac{1}{2\chi}\mathscr{Q}. \tag{10}$$

This equation gives $\Delta\phi^{\mathrm{I}}$ as a function of surface charge and the mixed-layer potential drop. The potential drop in semispace II is

$$\Delta\phi^{\mathrm{II}} = -2\ln\left[\frac{\zeta}{4\gamma}(\mathscr{Q} - \chi\Delta\phi^{\mathrm{int}}) + \sqrt{\frac{\zeta^2}{16\gamma^2}(\mathscr{Q} - \chi\Delta\phi^{\mathrm{int}})^2 + 1}\right] - \frac{1}{2}\Delta\phi^{\mathrm{int}} - \frac{1}{2\chi}\mathscr{Q}. \tag{11}$$

The sum of $\Delta\phi^{\mathrm{I}}$ and $\Delta\phi^{\mathrm{II}}$ is the overall potential drop $\Delta\phi$.

As a final equation to close the model, the surface charge on dividing surface IHP is related to the surface concentration of penetrating species by

$$\mathscr{Q} = n_{\mathrm{s}}(\Theta_{+,\mathrm{I}} - \Theta_{-,\mathrm{I}} + \Theta_{+,\mathrm{II}} - \Theta_{-,\mathrm{II}}). \tag{12}$$

This equation introduces a dimensionless quantity, the *saturation number*

$$n_{\mathrm{s}} = \frac{\Gamma_{\mathrm{T}} F^2 z^2}{RT\epsilon_0}\sqrt{\frac{\lambda^{\mathrm{I}}\lambda^{\mathrm{II}}}{\epsilon^{\mathrm{I}}\epsilon^{\mathrm{II}}}} = N_{\mathrm{A}}\Gamma_{\mathrm{T}} L_{\mathrm{B}}\sqrt{\lambda^{\mathrm{I}}\lambda^{\mathrm{II}}}, \tag{13}$$

where Γ_{T} represents the total molar surface concentration of available penetration sites, L_{B} is the Bjerrum length, and N_{A} is Avogadro's number. n_{s} thus represents the total number of available penetration sites contained on a surface of area $L_{\mathrm{B}}\sqrt{\lambda^{\mathrm{I}}\lambda^{\mathrm{II}}}$ in the inner plane. In the limit $n_{\mathrm{s}} \to 0$, the penetration equilibria become trivial and the system behaves as though it has a compact solvent layer between the two diffuse double layers. When n_{s} is nonzero, ions may enter the inner layer.

An estimate can be obtained for the total site concentration by computing the average number of solvent molecules per unit area in the inner layer. This is given to a first approximation by the mean of the pure-solvent concentrations multiplied by the inner-layer thickness d; this estimate results in $n_{\mathrm{s}} \approx 200$ for the system studied here. Su et al. [28] performed their analysis under conditions in which $n_{\mathrm{s}} \approx 6$.

The ITIES capacitance, C_{ITIES}, was obtained by numerical differentiation, through the definition

$$C_{\mathrm{ITIES}} = \left(\frac{\partial q^{\mathrm{II}}}{\partial\Delta\Phi}\right)_{T,p} = \epsilon_0\sqrt{\frac{\epsilon^{\mathrm{I}}\epsilon^{\mathrm{II}}}{\lambda^{\mathrm{I}}\lambda^{\mathrm{II}}}}\left(\frac{\partial\mathscr{Q}^{\mathrm{II}}}{\partial\Delta\phi}\right)_{T,p}. \tag{14}$$

In this equation, q^{II} is the total charge per unit superficial area from semispace II and $\mathscr{Q}^{\mathrm{II}}$ is its dimensionless form, defined similarly to $\mathscr{Q}$ in Eq. (3). The total semispace charge is the sum of the surface excess charge of diffuse layer II and the charges of the species from phase II on IHP,

$$\mathscr{Q}^{\mathrm{II}} = \frac{2\zeta}{\alpha}\sinh\left[-\frac{1}{4}\left(\Delta\phi^{\mathrm{int}} - \frac{\delta}{\chi}\mathscr{Q}\right) + \frac{1}{2}\Delta\phi^{\mathrm{II}}\right] + n_{\mathrm{s}}(\Theta_{+,\mathrm{II}} - \Theta_{-,\mathrm{II}}). \tag{15}$$

The first term describes a contribution of the diffuse layer and the second term represents a contribution of the charge on surface IHP.

Eqs. (1), (4), (9), and (12) give seven governing equations that contain seven unknowns: the surface charge $\mathcal{Q}$, the inner-layer potential drop $\Delta\phi^{\text{int}}$, four fractional surface coverages of ions, $\Theta_{+,\text{I}}$, $\Theta_{-,\text{I}}$, $\Theta_{+,\text{II}}$, and $\Theta_{-,\text{II}}$, and the fractional surface coverage of available sites, $\Theta_{*,\text{IHP}}$. The semispace potential drops in terms of which the penetration equilibria in Eq. (9) are expressed, $\Delta\phi^{\text{I}}$ and $\Delta\phi^{\text{II}}$, are dependent on $\mathcal{Q}$ and $\Delta\phi^{\text{int}}$ by Eqs. (10) and (11).

The capacitance of the ITIES is determined by several independently accessible dimensional parameters. Electrostatics are parameterized by the equivalent charges and stoichiometric numbers of ions, z and ν, the salt Debye lengths λ^j, the three dielectric constants ϵ^j, the bulk electrolyte concentrations c_0^j, the absolute temperature T, and the inner-layer thickness d. In the governing equations, the overall potential drop $\Delta\Phi$ may be fixed arbitrarily, as it would be in experiments. Penetration equilibria are parameterized by all of the aforementioned quantities, as well as the concentrations of pure solvent in phase j, $c_{\text{s}}^j = 1/a_{i,j}^{\theta}$, the four penetration free-energy barriers $\Delta G_{i,j}^{\text{IHP}}$, and the surface concentration of penetration sites, Γ_{T}. The penetration energies depend on the free energies of ion transfer, $\Delta G_i^{j,k}$, as well as one free parameter – the transfer fraction α.

To generate the data presented here, Eqs. (1), (4), (9), and (12) were solved for the seven variables $\mathcal{Q}$, $\Delta\phi^{\text{int}}$, and $\Theta_{i,j}$ over a range of the parameter $\Delta\phi$. These results were used to obtain $\mathcal{Q}^{\text{II}}$ as a function of $\Delta\phi$ with Eq. (15), which was then differentiated to compute the capacitance by Eq. (14). The problem can be reduced from seven dimensions to one; this streamlined computational procedure is presented in A. The derivative in the definition of capacitance was computed numerically by a finite-difference approximation; presented numerical results are accurate to the fifth significant digit.

2.2. Results

Fig. 3 shows the "three-phase" model capacitance response for the ITIES when the penetration barrier, $\Delta G_{i,j}^{\text{IHP}}$, is set to an identical value for all species. Each relevant parameter used to describe the system is listed in Table 1. Dielectric constants and solvent concentrations are reported for the pure solvents [30,40], and the neat inner-layer thickness was estimated from the experimental X-ray diffraction data provided by Luo et al. [1].

As previously discussed, the Verwey–Niessen theory can be obtained by taking $n_{\text{s}} \to 0$, which makes the adsorption equilibria trivial; the same results can alternatively be reached via infinite free-energy barriers to ionic penetration. The development by Su et al. [28] also follows as a limiting case of the three-phase model. Their results may be duplicated by taking χ and all but one of the $\Delta G_{i,j}^{\text{IHP}}$ to infinity and choosing a nonzero value of the saturation number, $n_{\text{s}} = 6.4$. Because comparison to familiar classical models is of primary interest here, this case is not shown in the following discussion.

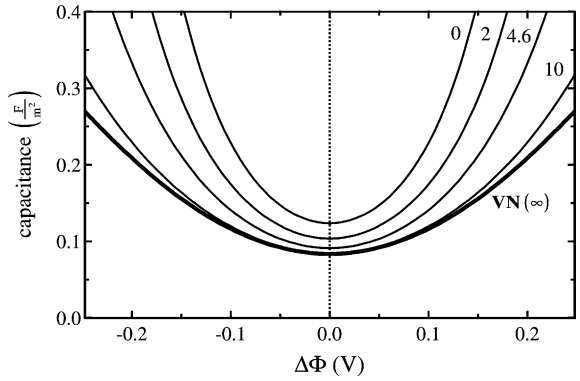

Fig. 3. Lower free-energy barriers to inner-layer ion penetration increase the capacitance. Results for the water/nitrobenzene ITIES at 0.01 M are shown by solid curves for several cases in which the penetration barrier is varied for all four ions. Each curve is labeled with the value of $\Delta G_{i,j}^{\text{IHP}}$ in kJ/mol. The Verwey–Niessen compact layer model (bold black line, VN) corresponds to an infinite barrier.

Table 1
Properties of the water/nitrobenzene (NB) ITIES used to generate Figs. 3–7

Phase II (water)		Phase I (nitrobenzene)	
ϵ^{II}	78.33	ϵ^{I}	34.82
c_{s}^{II}	55.3 M	c_{s}^{I}	9.20 M
c_0^{II}	0.01 M	c_0^{I}	0.01 M
λ^{II}	3.04 nm	λ^{I}	2.03 nm
ITIES			
ϵ^{int}	56.58	d	0.5 nm
Γ_{T}	3.23×10^{-5} mol/m^2	$-\frac{N_{\text{A}}e^2}{r\epsilon^{\text{int}}}$	~ -10 kJ/mol

The Debye lengths are reported at the listed concentration. For the salt, $\nu = 1$ and $z = 1$ equiv/mol. Dielectric constants are taken to be those of the pure solvents [30,40].

When the ionic penetration barriers are lowered (cf. Fig. 3) the system capacitance rises relative to the Verwey–Niessen curve. This rise can be understood by considering the length scales over which charge is distributed. In systems where ions are prevented from entering the inner layer, the charge is spread over a certain range that is reduced exponentially with increased polarization. If ions are allowed to enter the inner layer, the range of the charge distribution is shortened due to the charge contained in phase int. The resultant effect is a net increase of the system capacitance.

Gouy–Chapman predictions can be obtained as a limit of the model by taking $n_{\text{s}} \to 0$ and $\chi \to \infty$; the second condition corresponds to an inner layer of zero thickness. Results of the three-phase model are most

easily compared to the Gouy–Chapman theory by a Parsons–Zobel plot, which is shown in Fig. 4. In the plot, the inverse values of capacitances yielded by the model, $1/C_{\mathrm{ITIES}}$, are plotted against the inverse Gouy–Chapman values over concentrations ranging from 0.005 to 0.1 M. The points represent data obtained at three different values of the penetration barrier, which was set to be the same for all species.

Linear fits of the data in Fig. 4 demonstrate that when ions penetrate into the inner layer the apparent Stern-layer capacitance given by the intercepts of the linear extrapolation is reduced. As the adsorption barrier lowers, the apparent compact layer capacitance may even become negative. The intercept, however, is not reached by the full curve. In reality, as concentration rises, the data at null penetration barrier begin to deviate upward from the fit and eventually intercept the vertical axis at a value of approximately 0.15 m^2/F. However, the data points in the plot are presented over a practical range to show that experimental results gathered at reasonable concentrations may yield aphysical "Stern-layer" capacitances when penetration occurs.

Upward deviation from linearity in a Parsons–Zobel plot, as observed in the three points at the left of the null penetration-barrier curve in Fig. 4, is a signature of ion penetration into the inner layer. This deviation decreases as the penetration barrier is increased. When there is no penetration, the Verwey–Niessen theory gives an ideally straight Parsons–Zobel line. Relaxing the barrier increases penetration and thereby enhances the deviation "upward". Thus, the larger the deviation observed on an experimental curve, the greater the expected penetration of ions. This not new conceptually, as distortions of straightness in Parsons–Zobel plots are typically considered to be a signature of specific adsorption.[3]

In addition, Fig. 4 shows that when penetration barriers are near 4.6 kJ/mol for all species, the result of the three-phase model corresponds nearly exactly to the result of the Gouy–Chapman prediction. In the following comparison of model results to experimental data this is found to be an appropriate magnitude for the barriers, explaining to some extent how the Gouy–Chapman model has such great success at fitting experimental results [30,8] while neglecting the presence of an inner layer.

[3] At metal/electrolyte interfaces, the deviation typically goes down. [41–46] show that this can be attributed to the interference of structural effects and correlations in the Debye plasma of electrolytes. This theory predicted "downward" deviation because the effective dielectric constant of water near the metal surface was lower than in the bulk. In the "three-phase" model there is also no compact Stern layer, as ions may penetrate. But if the aqueous part is taken as an analogue of the metal electrode, and the organic phase as one of the bulk solution, the effective dielectric constant of the inner layer is higher than of the bulk organic solvent. Thus it is natural to expect deviation "up" on a Parsons–Zobel plot.

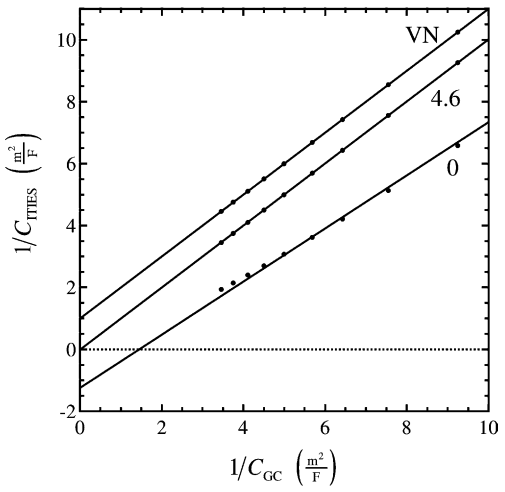

Fig. 4. Inner-layer penetration suppresses the apparent capacitance of the inner layer. Parsons–Zobel plot of the model results over a range of penetration barriers. Each curve was obtained by a linear fit of data over ten solution compositions ranging from 0.005 to 0.1 M, spaced evenly with respect to the square root of concentration. The curves are labeled with the value of $\Delta G_{i,j}^{\mathrm{IHP}}$ for all species; $\Delta G_{i,j}^{\mathrm{IHP}} = 4.6$ kJ/mol coincides almost exactly with the Gouy–Chapman prediction.

When all of the penetration energies are equal, the qualitative features of the capacitance response are similar to those yielded by the classical theories: the capacitance is symmetric about zero polarization, and increases exponentially with polarizations of either sign. More dramatic effects occur when the penetration barriers differ among ions. Fig. 5 shows the capacitance response when the penetration barrier is removed for a single species; the result of the Verwey–Niessen theory is shown on the plot for comparison.

If the penetration barrier is lowered for a single ion, the capacitance response becomes asymmetric with respect to potential and the capacitance minimum shifts to the right or left. Fig. 5 demonstrates this shift for each species. If cations from the water phase or anions from the organic phase penetrate the inner layer, the capacitance minimum shifts to the left; a shift to the right occurs if either of the other two species penetrates.

To understand the capacitance-minimum shifts, consider the case when cations from the water phase are allowed to penetrate the inner layer. A positive polarization drives aqueous cations toward the inner layer and a negative polarization drives them away. Because aqueous cations may enter phase int, the charge in the aqueous phase is distributed over a shorter region than the compact-layer theory predicts at positive polarizations. At negative polarizations, aqueous cations are driven away from the interface and the capacitance response returns to that predicted by the compact-layer theory. The overall result is an asymmetric capacitance curve with a minimum shifted to the left of zero polarization. Similar reasoning can be applied to describe the shifts of the other curves qualitatively.

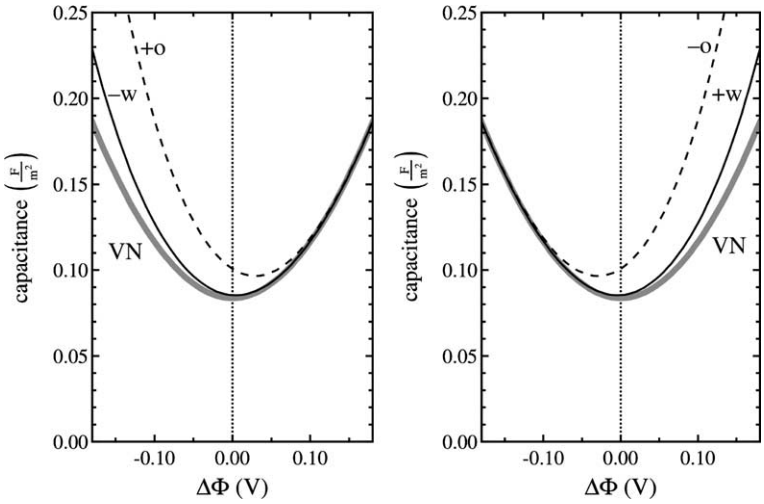

Fig. 5. Ion penetration induces asymmetry and shifts the capacitance minimum. Capacitance responses when the penetration barrier is lowered to $\Delta G_{i,j}^{\mathrm{IHP}}$ for a single species and the rest cannot enter the inner layer, $\Delta G_{i,j}^{\mathrm{IHP}} \to \infty$. The gray curve shows the Verwey–Niessen result corresponding to a compact solvent layer. Curves are labeled by ion; solid lines correspond to aqueous ions and dashed lines to organic ions.

Fig. 5 also shows that aqueous ion penetration leads to a lower overall rise in capacitance than organic ion penetration. This discrepancy can be explained by the differences in dielectric constants between the inner layer and the solvents flanking it on either side. Water has a much higher dielectric constant than NB, and phase int has a dielectric constant of an intermediate value. If organic ions penetrate the inner layer, they enter a region with a higher dielectric constant than the double layer they leave; the opposite situation holds for aqueous ions. Thus, the net contribution to the capacitance response is higher when organic ions enter the inner layer and lower when aqueous ions penetrate.

It should be noted that the capacitance features discussed above (asymmetry and a shift of the minimum) were predicted earlier within a perturbation approach [4]. The important advantage of the present theory is that it allows the analysis to go beyond the range of small perturbations and to consider the large deviations from the Gouy–Chapman and Verwey–Niessen results that have been observed experimentally.

2.3. Comparison with experiments

To test the validity of the physical approximations employed in its development, the model results were compared to experimental data from an exemplary ITIES. Samec et al. [31] measured the capacitance–voltage response of a concentration-balanced ITIES containing aqueous sodium bromide (NaBr) and tetrabutylammonium tetraphenylborate (TBATPB) in NB at 298 K by taking the slopes of galvanostatic transients. Because the free energies of transfer for this system are well known, the data could be used to determine the physical accuracy of this model. The relevant parameters that describe this experimental system are listed in Table 2. Ionic free energies of transfer were taken from the summary provided in [29] and from Samec et al. [30]. The model results are compared with the experimental data in Fig. 6; results provided by the Gouy–Chapman and Verwey–Niessen theories are presented on the same figure for comparison.

Table 2
Properties of aqueous NaBr and tetraphenylammonium tetraphenylborate (TBATPB) in NB used to generate Fig. 6

(Aqueous NaBr)/(TBATPB in NB)			
$\Delta G_{+}^{\mathrm{II,I}}$	32 kJ/mol	$\Delta G_{+}^{\mathrm{I,II}}$	26 kJ/mol
$\Delta G_{-}^{\mathrm{II,I}}$	22 kJ/mol	$\Delta G_{-}^{\mathrm{I,II}}$	35 kJ/mol

Literature values for the free energies of transfer were obtained from [29] and [30].

The experimental data show the characteristic features of ion penetration; they are asymmetric about zero overpotential. Fig. 6 shows the results of the basic model at an electrolyte concentration of 0.01 M. Model results lie significantly closer to the experimental data than the predictions of either the Gouy–Chapman or the Verwey–Niessen theories. The Verwey–Niessen model consistently underpredicts the experimental data, and the Gouy–Chapman model, while providing a better estimate than the Verwey–Niessen theory, fails to capture the asymmetry of the capacitance response.

The data are fit well with a transfer fraction of $\alpha = 0.11$. The fact that $\alpha < 0.5$ is physically reasonable. The interface of two liquids is soft; as ions from one phase approach it, they cause protrusions into the opposing phase. Thus, the free energy at surface IHP, which has fixed position, is effectively lower, resulting in a smaller transfer fraction. A value of $\alpha = 0.11$ yields penetration energies of the order of 2–4 kJ/mol for all species. These energies are in the

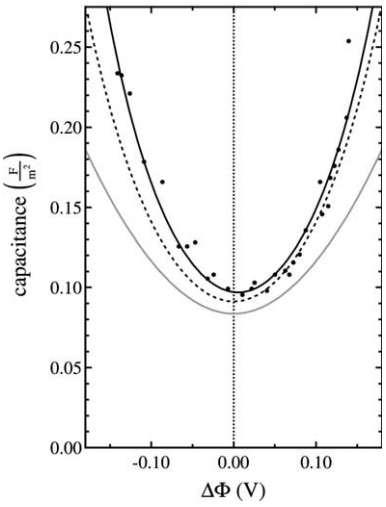

Fig. 6. The "three-phase" model rationalizes asymmetry in an experimental capacitance curve. Comparison of the model with no solute–solute interactions to experimental data from the (aqueous NaBr)/(TBATPB in NB) system at 0.01 M. The fit was obtained with appropriate free energies of transfer and the single transfer fraction $\alpha = 0.11$ for all ions. Solid circles represent data, the gray curve depicts the Verwey–Niessen theory, the dashed curve shows the Gouy–Chapman theory, and the black curve is the model result. Experimental data are reproduced from Samec et al. [31].

range where ionic penetration leads capacitances to have magnitudes of the order predicted by the Gouy–Chapman theory.

3. Incorporating ion pairing

3.1. Modification of the model

Phenomenological considerations by Cheng et al. [47] and Pereira et al. [48] and simulations by Schmickler [21] also suggest that solute–solute interactions may play a role at the inner layer. To take these interactions into account in the model, the penetration-barrier free energy given by Eq. (5) may be modified by an energetic correction [49,50],

$$\Delta G_{i,j}^{\mathrm{IHP}} = \alpha \Delta G_i^{j,k} + \sum_{k=1}^{2} \sum_{m=1}^{2} \beta_{i,km} \Theta_{k,m}, \tag{16}$$

where $\beta_{i,km}$ denotes the specific-interaction energetic contributions between species i and species k from phase m on surface IHP, and $\Theta_{i,j}$ denotes the fractional surface penetration of species i native to phase j on dividing surface IHP. These interactions can be attributed to forces that arise when ions are proximate on the lattice (what are often called "discreteness-of-charge" effects in the double-layer theory). In the model, $\beta_{i,km}$ is zero for species of like charge, in line with the Brønsted principle of specific ion interactions [51]. Simply put, ions of like charge rarely meet at the interface due to their electrostatic repulsion; they are rarely nearest neighbors at IHP and their interactions can be neglected. The interaction parameters are taken to be symmetric as in the Brønsted theory – the interaction energy between species i and species k from phase m is the same as that between species k from phase m and species i. The order of the ion-pairing energies can be roughly estimated by the classical electrostatic coulomb energy of two oppositely charged particles in contact,

$$\beta_{i,km} \sim -\frac{N_{\mathrm{A}} e^2}{4\pi r \epsilon^{\mathrm{eff}} \epsilon_0}, \tag{17}$$

in which r denotes the mean of the two ionic radii, ϵ^{eff} is the effective dielectric constant of the medium when ions are proximate, and e is an elementary charge. Avogadro's number N_{A} is included to translate the estimate into a molar energy. The magnitude of this estimate for the water/NB system is included in Table 1.

The cation/anion IHP interaction energies $\beta_{i,km}$ add four free parameters to the model and lead $\Delta G_{i,j}^{\mathrm{IHP}}$ to depend on coverage. When interactions are taken into account, the governing equations must be solved simultaneously for the charge, coverages, and inner-layer potential drop. To generate the results presented below, the governing system was solved by a seven-dimensional Newton–Raphson procedure. The transfer fraction α is set to zero to eliminate the penetration barrier and enhance the effects of solute–solute interactions.

3.2. Results

Capacitance responses at larger applied potentials, when available penetration sites become limiting and solute–solute interactions occur in the inner layer, are shown in Fig. 7. The figure shows the capacitance when interionic attraction in the interfacial region is described by Eq. (16), which leads to a Frumkin isotherm when interactions occur. When included, the interaction energies $\beta_{i,jm}$ are set to the order estimate given in Table 1. To amplify the effect of ion interactions, α is set to zero, which corresponds to the absence of barriers to ion penetration into the inner layer. Two ions are allowed to pair in each case shown in the figure; the dashed curves are labeled with the species that are allowed to form pairs, and the gray curves show the case where there is no penetration barrier and no pairing.

One feature should be noted immediately from Fig. 7: available penetration sites become limiting at very high applied potentials. This effect is clear from the inflection points in the gray curve at $\sim\pm 0.25$ V. When the potential bias becomes sufficiently large, the available sites for ion penetration become saturated. Capacitance begins to fall because ions are no longer permitted to leave the diffuse double layers and reach the inner layer. As polarization rises, the portion of the overall potential drop that occurs across the inner region increases; even-

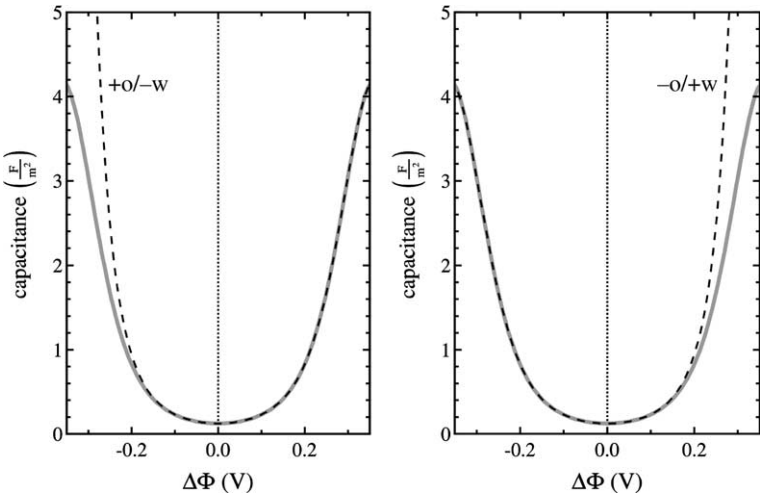

Fig. 7. Ion pairing can asymmetrically effect the capacitance at large applied potentials without shifting its minimum. Capacitance response when interactions exist between species of opposite charge at the inner layer. The transfer fraction α is set to zero. Curves are labeled with the species that are allowed to interact, for which $\beta_{i,jm} = -10$ kJ/mol in each case. The bold gray line corresponds to $\beta_{i,jm} = 0$ for all species; it coincides with the response when interactions occur between ions from the same phase.

tually, the inner layer comes to dominate the capacitance.

Interactions between species from the same phase do not affect the capacitance response; the curves for aqueous cation–anion interactions and organic cation–anion interactions coincide with the zero-interaction curve and are not shown in Fig. 7. This result owes to the fact that when the double layer is polarized, the concentration of one ion at OHP rises exponentially and that of the other falls exponentially. Interaction energetics in the inner layer cannot overcome the electrostatic response of the double layer, and therefore no signature of ion pairing is observed in the capacitance.

However, at high polarizations the capacitance is significantly affected by interactions between oppositely charged species from different phases at the inner layer. In Fig. 7, ion–ion interactions manifest as an asymmetry in the capacitance response without a corresponding translation of the capacitance minimum. The interactions affect results only under applied potentials when both species are driven toward the interface. Thus, the aqueous cation/organic ion interactions cause the capacitance to increase with positive polarizations, and aqueous anion/organic cation interactions cause it to increase with negative ones. At high applied potentials, the contribution of species interactions obscures the effects of site limitation.

3.3. Does ion pairing appear in the data?

Now that interactions have been considered, it is appropriate to return to the data presented in Fig. 6. To generate the figure, $\beta_{i,km}$ were neglected and the transfer fraction α was adjusted to fit the data. The model provides an excellent fit over the entire range of potentials, save for a few outlying points. In theory, the discussion provided in this section demonstrates that the deviating point at large positive potential could be matched by the inclusion of surface interactions between Na^+ and TPB^- ions. However, the interaction energies required to match the experimental data were found to be significantly higher than the Coulomb-energy estimate; this adjustment of the model was therefore deemed inappropriate. One possibility that would account for this issue is that the free energy of interaction depends on potential, as postulated by Higgins and Corn to describe surfactant adsorption at the interface [52]. Also, nonlocal electrostatic effects may occur at very short distances and dramatically increase the energies of interionic interactions [41].

4. Concluding remarks

A three-phase phenomenological model has been proposed to account for ion penetration and interactions at the inner layer of an ITIES. It provides a theoretical justification for experimentally observed asymmetries in the capacitance–voltage response that cannot be provided by the Gouy–Chapman or Verwey–Niessen theories. The model incorporates penetration energetics through independently measurable free energies of ion transfer, which are scaled by a fraction α to account for the fact that penetrating species do not have to overcome their entire transfer energy to enter the mixed inner layer between solvents.

The Gouy–Chapman and Verwey–Niessen theories can both be obtained as limiting cases of the model. When mixed-layer penetration occurs, it tends to raise the system capacitance above the Verwey–Niessen limit.

If the penetration energy of a single species differs from the others, it causes the capacitance minimum to shift and the curve becomes asymmetric with respect to potential about its minimum. Interactions between ions at the inner layer also affect the capacitance response; they lead to asymmetry of the capacitance curves without a corresponding shift in the minimum. However, the effects of ion interactions only appear at large polarizations.

Experimental data were fit by the theory with the single-parameter model given by Eq. (18). The results correctly predict the deviation of the capacitance–voltage curves from the idealized Gouy–Chapman theory and agree with data significantly better than the results of the Verwey–Niessen compact layer model. Thus, limited species penetration into the mixed layer is a physically reasonable hypothesis. Application of this principle can explain the curious features common to most experimental results and rationalize perplexing negative or zero values of the inverse "compact-layer capacitances" at interfaces between immiscible electrolytes.

Acknowledgments

The authors are thankful to Hubert Girault (EPFL) and Bob Samec (Heyrovsky Institute) for useful discussions. Special thanks are due to Sasha Kuznetsov (Frumkin Institute) for his valuable insights during the developmental stages of the project. The whole work was made possible by the generous support of the Leverhulme Trust, Grant No. F/07058/P.

Appendix A.

The seven governing equations may be solved directly by seven-dimensional New-ton-Raphson iteration. However, the problem can be reduced to one dimension when $\beta_{i,km}$ is zero or at moderate polarizations when the impact of the interaction contribution to capacitance is small. The $\Delta G_{i,j}^{\mathrm{IHP}}$ are then constant with respect to the surface coverage of ions. When the equilibrium constants $\mathscr{K}_i^j$ are independent of coverage, the governing system may be simplified by substitution of the adsorption equilibrium expressions into Eq. (4) and insertion of the result into Eq. (12). This yields the single master equation

$$\mathscr{Q}(\mathscr{Q},\Delta\phi^{\mathrm{int}}) = \frac{n_{\mathrm{s}}\varpi(\mathscr{Q},\Delta\phi^{\mathrm{int}})}{1+\mathscr{K}(\mathscr{Q},\Delta\phi^{\mathrm{int}})}, \tag{18}$$

where the functions ϖ and $\mathscr{K}$ are given by

$$\varpi(\mathscr{Q},\Delta\phi^{\mathrm{int}}) = \mathscr{K}_{+}^{\mathrm{I}}\mathrm{e}^{-\Delta\phi^{\mathrm{I}}} - \mathscr{K}_{-}^{\mathrm{I}}\mathrm{e}^{\Delta\phi^{\mathrm{I}}} + \mathscr{K}_{+}^{\mathrm{II}}\mathrm{e}^{\Delta\phi^{\mathrm{II}}} - \mathscr{K}_{-}^{\mathrm{II}}\mathrm{e}^{-\Delta\phi^{\mathrm{II}}}, \tag{19}$$

$$\mathscr{K}(\mathscr{Q},\Delta\phi^{\mathrm{int}}) = \mathscr{K}_{+}^{\mathrm{I}}\mathrm{e}^{-\Delta\phi^{\mathrm{I}}} + \mathscr{K}_{-}^{\mathrm{I}}\mathrm{e}^{\Delta\phi^{\mathrm{I}}} + \mathscr{K}_{+}^{\mathrm{II}}\mathrm{e}^{\Delta\phi^{\mathrm{II}}} + \mathscr{K}_{-}^{\mathrm{II}}\mathrm{e}^{-\Delta\phi^{\mathrm{II}}}. \tag{20}$$

The quantities $\Delta\phi^{\mathrm{I}}$ and $\Delta\phi^{\mathrm{II}}$ can be obtained as functions of $\mathscr{Q}$ and $\Delta\phi^{\mathrm{int}}$ through Eqs. (10) and (11); Eq. (18) thus represents a transcendental equation that gives $\mathscr{Q}$ as a function of $\Delta\phi^{\mathrm{int}}$.

Transcendental master equation (18) can be solved to high precision in a few iterations by Newton's method. Substitution of Eq. (9) into (12) shows

$$\Theta_{*,\mathrm{IHP}} = \frac{\mathscr{Q}}{\varpi n_{\mathrm{s}}}. \tag{21}$$

When $\mathscr{K}_i^j$ is constant with respect to $\Theta_{i,j}$, each ion coverage in Eq. (9) is a function of $\mathscr{Q}$ and $\Delta\phi^{\mathrm{int}}$ only, through algebraic equations (10), (11), (19), and (21). Eq. (1) can be also be used to retrieve the overall potential drop $\Delta\phi(\mathscr{Q},\Delta\phi^{\mathrm{int}})$. The problem can thus be solved efficiently by specification of $\mathscr{Q}$ when $\mathscr{K}_i^j$ is constant, and the application of a far slower seven-dimensional Newton–Raphson procedure is unnecessary. With this computational method, capacitance curves may be obtained more rapidly.

References

[1] G.M. Luo, S. Malkova, S.V. Pingali, D.G. Schultz, B.H. Lin, M. Meron, T.J. Graber, R. Bebhardt, P. Vanysek, M.L. Schlossman, X-ray studies of the interface between two polar liquids: neat and with electrolytes, Faraday Discuss. 129 (2005) 23.
[2] W. Schmickler, The influence of the ions on the capacity of liquid–liquid interfaces, J. Electroanal. Chem. 467 (1–2) (1999) 203.
[3] I. Benjamin, Molecular structure and dynamics at liquid–liquid interfaces, Annu. Rev. Phys. Chem. 48 (1997) 407.
[4] L.I. Daikhin, A.A. Kornyshev, M. Urbakh, Ion penetration into an "unfriendly medium" and the double layer capacitance of the interface between two immiscible electrolytes, J. Electroanal. Chem. 500 (1–2) (2001) 461.
[5] G.L. Gouy, Sur la constitution de la charge électrique a la surface d'un électrolyte, J. Phys. 9 (1910) 457.
[6] D.L. Chapman, A contribution to the theory of electrocapillarity, Philos. Mag. 25 (1913) 457.
[7] O. Stern, Zur theorie der elektrolytischen doppelschicht, Z. Elektrochem. 30 (1924) 508.
[8] H.H. Girault, D.J. Schiffrin, Electrochemistry of liquid–liquid interfaces, in: A.J. Bard (Ed.), Electroanalytical Chemistry, vol. 15, Marcel Dekker, New York, 1985, p. 1.
[9] E.J.W. Verwey, K.F. Niessen, The electrical double layer at the interface of two liquids, Philos. Mag. 28 (1939) 435.
[10] C. Gavach, P. Seta, B. d'Epenoux, The double layer and ion adsorption at the interface between two non miscible solutions part I. Interfacial tension measurements for the water–nitrobenzene tetraalkylammonium bromide systems, J. Electroanal. Chem. 83 (2) (1977) 225.
[11] L. Murtomäki, K. Kontturi, D.J. Schiffrin, Some remarks on the double layer correction to the kinetics of ion transfer at the interface of immiscible electrolytes, J. Electroanal. Chem. 474 (1) (1999) 89.
[12] L.I. Daikhin, M. Urbakh, Double layer capacitance and a microscopic structure of electrified liquid–liquid interfaces, J. Electroanal. Chem. 560 (2003) 59.
[13] I. Benjamin, Pitfalls, challenges and promise of molecular simulations of liquid interfaces, Lecture, Imperial College, London, December 2004

[14] R. Parsons, F.G.R. Zobel, The interphase between mercury and aqueous sodium dihydrogen phosphate, J. Electroanal. Chem. 9 (5–6) (1965) 333.
[15] A.A. Kornyshev, Solvation of a metal surface, in: R.R. Dogonadze, E. Kálmán, A.A. Kornyshev, J. Ulstrup (Eds.), The Chemical Physics of Solvation, Part C, Elsevier, Amsterdam, 1985, p. 355.
[16] G.L. Richmond, Molecular bonding and interactions at aqueous surfaces as probed by vibrational sum frequency spectroscopy, Chem. Rev. 102 (8) (2002) 2693.
[17] P. Brevet, Nonlinear optics at liquid–liquid interfaces, in: A.G. Volkov (Ed.), Surfactant Science Series 95: Liquid Interfaces in Chemical, Biological, and Pharmaceutical Applications, Marcel Dekker, USA, 2001, p. 123.
[18] A. Trojanek, P. Krtil, Z. Samec, Quasi-elastic laser light scattering from thermally excited capillary waves on liquid/liquid interfaces part1: effects of adsorption of hexadecyltrimethylamchloride chloride at water/1,2-dichloroetinterface interface, J. Electroanal. Chem. 517 (1–2) (2001) 77.
[19] K. Schweighofer, I. Benjamin, Transfer of a tetramethylammonium ion across the water–nitrobenzene interface: potential of mean force and nonequilibrium dynamics, J. Phys. Chem. A 103 (49) (1999) 10274.
[20] W. Schmickler, A lattice–gas model for ion pairing at liquid–liquid interfaces, J. Electroanal. Chem. 483 (1–2) (2000) 18.
[21] W. Schmickler, Structure of liquid/liquid interfaces from a lattice gas model, J. Electroanal. Chem. 564 (1–2) (2004) 239.
[22] L.I. Daikhin, A.A. Kornyshev, M. Urbakh, Capillary waves at soft electrified interfaces, J. Electroanal. Chem. 483 (2000) 68.
[23] G.M. Torrie, J.P. Valleau, Double layer structure at the interface between two immiscible electrolyte solutions, J. Electroanal. Chem. 206 (1986) 69.
[24] Z. Samec, V. Mareček, D. Homolka, The double layer at the interface between two immiscible electrolyte solutions part II, J. Electroanal. Chem. 187 (1985) 31.
[25] C.M. Pereira, W. Schmickler, F. Silva, M.J. Sousa, On the capacity of liquid–liquid interfaces, Chem. Phys. Lett. 268 (1–2) (1997) 13.
[26] T. Huber, O. Pecina, W. Schmickler, The influence of the ions on the capacity of liquid–liquid interfaces, J. Electroanal. Chem. 467 (1–2) (1999) 203.
[27] C.M. Pereira, W. Schmickler, F. Silva, M.J. Sousa, Ion association at liquid–liquid interfaces, J. Electroanal. Chem. 436 (1–2) (1997) 9.
[28] B. Su, N. Eugster, H. Girault, Simulations of the adsorption of ionic species at polarisable liquid–liquid interfaces, J. Electroanal. Chem. (in press)
[29] A.A. Kornyshev, A.G. Volkov, On the evaluation of standard Gibbs energies of ion transfer between two solvents, J. Electroanal. Chem. 180 (1984) 363.
[30] Z. Samec, D. Homolka, V. Mareček, L. Kavan, Charge transfer between two immiscible electrolyte solutions, J. Electroanal. Chem. 145 (1983) 213.
[31] Z. Samec, V. Mareček, D. Homolka, Double layers at liquid/liquid interfaces, Faraday Discuss. Chem. Soc. 77 (1983) 197.
[32] T. Kakiuchi, M. Senda, Polarizability and electrocapillary measurements of the nitrobenzene water interface, Bull. Chem. Soc. Japan 56 (5) (1983) 1322.
[33] L.Q. Hung, E. Makrlik, Thermodynamics of transfer of some univalent ions from the aqueous phase into the nitrobenzene phase of a 2-phase water nitrobenzene extraction system, J. Electroanal. Chem. 158 (2) (1983) 269.
[34] J. Koryta, Theory and applications of ion-selective electrodes, part III, Anal. Chim. Acta 111 (911) (1979) 1.
[35] B. Hundhammer, T. Solomon, Determination of standard Gibbs energies of transfer of ions across the water chlorobenzene and nitrobenzene interface, J. Electroanal. Chem. 169 (1–2) (1983) 311.
[36] T. Osakai, H. Katano, K. Maeda, S. Himeno, A. Saito, A hydrophobicity scale of heteropolyanions and isopolyanions based on voltammetric studies of their transfer at the nitrobenzene water interface, Bull. Chem. Soc. Japan 66 (4) (1993) 1111.
[37] S.M. Ulmeanu, H. Jensen, Z. Samec, G. Bouchard, P.A. Carrupt, H.H. Girault, Cyclic voltammetry of highly hydrophilic ions at a supported liquid membrane, J. Electroanal. Chem. 530 (1–2) (2002) 10.
[38] Q.Z. Chen, K. Iwamoto, M. Seno, Transfer of alkali-metal ions across the water–nitrobenzene interface facilitated by poly(oxyethylene) dodecyl ethers, Electrochim. Acta 37 (4) (1992) 643.
[39] J. Newman, K. Thomas-Alyea, Electrochemical Systems, 3rd ed., Wiley, Hoboken, NJ, 2004.
[40] R.C. Weast (Ed.), CRC Handbook of Chemistry and Physics, 59th ed., CRC Press, West Palm Beach, FL, 1978, p. E61.
[41] A.A. Kornyshev, J. Ulstrup, Nonlocal electrostatics of solvation, in: R.R. Dogonadze, E. Kálmán, A.A. Kornyshev, J. Ulstrup (Eds.), The Chemical Physics of Solvation, Part C, Elsevier, Amsterdam, 1985, p. 77.
[42] M.A. Vorotyntsev, V. Izotov, A.A. Kornyshev, Differential capacity of the double layer in dilute solutions, Elektrokhimiya 19 (1983) 407.
[43] A.A. Kornyshev, M.A. Vorotyntsev, Nonlocal dielectric response of the electrode/solvent interface in the double layer problem, Can. J. Chem. 59 (1981) 2031.
[44] A.A. Kornyshev, J. Ulstrup, Solvent structural effects on the diffuse double layer, Chem. Scripta 25 (1) (1985) 58.
[45] A.A. Kornyshev, J. Ulstrup, Solvent structural effects on the deviation from linear Parsons–Zobel plots with increasing electrolyte concentration, J. Electroanal. Chem. 183 (1–2) (1985) 387.
[46] L. Blum, D. Henderson, R. Parsons, The mean spherical approximation capacitance of the double-layer for an electrolyte at high-concentration, J. Electroanal. Chem. 161 (2) (1984) 389.
[47] Y. Cheng, V.J. Cunnane, D.J. Schiffrin, L. Murtomäki, K. Kontturi, Interfacial capacitance and ionic association at electrified liquid/liquid interfaces, J. Chem. Soc., Faraday Trans. 87 (1) (1991) 107.
[48] C.M. Pereira, F. Silva, M.J. Sousa, K. Kontturi, L. Murtomäki, Capacitance and ionic association at the electrified oil/water interface: the effect of the oil phase, J. Electroanal. Chem. 509 (2) (2001) 148.
[49] A.N. Frumkin, V.S. Bagotzky, Z.A. Iofa, B.N. Kabanov, Kinetika Elektrodnykh Protsessov, Moskovskii Univ., Moscow, 1952.
[50] M. Nauka, B.B. Damaskin, V.V. Batrakov, Adsorption of Organic Compounds on Electrodes, Springer, Berlin, 1975.
[51] J.N. Brønsted, Studies on solubility. IV. The principle of the specific interaction of ions, J. Am. Chem. Soc. 44 (1922) 877.
[52] D.A. Higgins, R.M. Corn, 2nd harmonic-generation studies of adsorption at a liquid–liquid electrochemical interface, J. Phys. Chem. 97 (2) (1993) 489.